Cyanoplatinate Halides – Synthesis, Crystal Structure Analyses and Vibrational Spectroscopy of Compounds $A_2[Pt(CN)_4X_2]$ (A = Rb, Cs; X = Cl, Br, I)

Claus Mühle, Jürgen Nuss, Robert E. Dinnebier, and Martin Jansen

Max-Planck-Institut für Festkörperforschung, Heisenbergstraße 1, 70569 Stuttgart, Germany

Reprint requests to Prof. Dr. Dr. h. c. M. Jansen. Fax: +49(0)711 6891502.
E-mail: M.Jansen@fkf.mpg.de

Z. Naturforsch. **2010**, *65b,* 1066 – 1072; received May 21, 2010

Crystal structures of the cyanoplatinates $A_2[Pt(CN)_4X_2]$ (A = Rb, Cs; X = Cl, Br, I) have been determined by single-crystal analysis and X-ray powder diffraction. The compounds were synthesized by metathesis from $Ba[Pt(CN)_4] \cdot 4\ H_2O$ and alkali metal sulfates, and by subsequent oxidation with the respective halogens. The crystals were grown by slowly concentrating respective aqueous solutions. The Pt^{IV} cations are octahedrally coordinated by four cyanide ligands and two halogen atoms, the latter being located in *trans* positions. *$Rb_2[Pt(CN)_4Cl_2]$*: triclinic, $P\bar{1}$ (Z = 2), a = 6.7779(2), b = 9.3149(3), c = 9.6707(3) Å, α = 89.37(0), β = 76.05(0), γ = 72.98(0)°, V = 565.42(2) Å^3, N'_{hkl}= 5616, $R(F)_{N'}$ = 0.0273; *$Rb_2[Pt(CN)_4I_2]$*: monoclinic, $P2_1/c$ (Z = 2), a = 7.4239(2), b = 9.2486(2), c = 9.1189(2) Å, β = 107.22(3)°, V = 598.04(6) Å^3, N'_{hkl} = 2917, $R(F)_{N'}$ = 0.0295; *$Cs_2[Pt(CN)_4I_2]$*: monoclinic, $P2_1/c$ (Z = 2), a = 7.6740(4), b = 9.5397(5), c = 9.3474(5) Å, β = 106.46(0)°, V = 656.3(2) Å^3, Z = 2, N'_{hkl} = 2738, $R(F)_{N'}$ = 0.0283; *$Cs_2[Pt(CN)_4Cl_2]$*: monoclinic, $C2/c$ (Z = 4), a = 17.947(4), b = 7.395(2), c = 12.031(3) Å, β = 131.904(1)°, V = 1188.4(5) Å^3, R-wp = 2.77; *$Cs_2[Pt(CN)_4Br_2]$*: monoclinic, $C2/c$ (Z = 4), a = 18.404(1), b = 7.2819(5), c = 12.4156(8) Å, β = 132.156(1)°, V = 1233.5(1) Å^3, N'_{hkl} = 2566, $R(F)_{N'}$ = 0.0268. All compounds were characterized by differential thermal analysis, thermogravimetry, and infrared and Raman spectroscopy.

Key words: Platinum, Cyanides, Crystal Structures, X-Ray Scattering, Vibrational Spectroscopy

Introduction

Platinum in its most common oxidation states of +II and +IV displays preferably square-planar or octahedral coordination geometries, respectively. Oxidation of cyanoplatinate complexes by halogens has been known for more than 150 years [1], and the prototype of partially oxidized $Pt^{+2.33}$ in $K_2[Pt(CN)_4Br_{0.33}] \cdot 3\ H_2O$ has been extensively studied and is well characterized by the original work of Krogmann [2, 3], and further investigations by Zeller [4]. A characteristic feature of the atomic structure of cyanoplatinates(II) is the presence of columns built by Pt in a square-planar coordination of cyanide groups. The Pt atoms approach each other realizing distances as short as 2.88 Å, which is only slightly longer than in metallic platinum (2.77 Å), suggesting one-dimensional metallic character and relatively high electron conductivity due to overlap of only partially filled Pt d_{z^2} orbitals. Since Krogmann's pioneering work, amazing physical-structural correlations in this class of compounds have been revealed by Williams [5], who studied also the crystal structures of $Rb_2[Pt(CN)_4Cl_{0.33}] \cdot 3\ H_2O$ [6] and $Cs_2[Pt(CN)_4Cl_{0.30}]$ [7] and their electrical properties [8]. A recent overview was given in 2009 [9], addressing the potential for the development of sensors and other technological applications using platinum polymers with short Pt–Pt distances. Partly oxidized cyanoplatinate halides are obtained from mixtures of the tetracyanoplatinate and the fully oxidized platinum halide complex in aqueous solution, and it appeared desirable to also know the crystal structures of compounds $A_2[Pt(CN)_4X_2]$ (A = alkali metal, X = halogen) and of related series of oxidation products of cyanoplatinates which are precursors for the one-dimensional complexes. So far, only the crystal structures of $Na_2[Pt(CN)_4Br_2] \cdot 2\ H_2O$ [10] and $Rb_2[Pt(CN)_4Br_2]$ [11] had been reported a few years ago, and we determined the structures of the potassium cyanoplatinate halides [12] and the hydrogen peroxide adducts $A_2[Pt(CN)_4] \cdot H_2O_2$ (A = alkali metal) [13].

Table 1. Crystallographic data and data collection from single-crystal measurements.

	$Rb_2[Pt(CN)_4Cl_2]$	$Cs_2[Pt(CN)_4Br_2]$	$Rb_2[Pt(CN)_4I_2]$	$Cs_2[Pt(CN)_4I_2]$
M_r, g mol^{-1}	541.01	724.81	723.91	818.79
Temperature, K	298(2)	298(2)	298(2)	298(2)
Crystal size, mm^3	0.15 × 0.18 × 0.25	0.25 × 0.15 × 0.10	0.30 × 0.25 × 0.20	0.25 × 0.20 × 0.12
Crystal system	triclinic	monoclinic	monoclinic	monoclinic
Space group (no.); Z	$P\bar{1}$ (2); 2	$C2/c$ (15); 4	$P2_1/c$ (14); 2	$P2_1/c$ (14); 2
a, Å	6.7779(2)	18.404(1)	7.4232(5)	7.6740(4)
b, Å	9.3149(3)	7.2819(5)	9.2468(6)	9.5397(5)
c, Å	9.6707(3)	12.4156(8)	9.1165(6)	9.3474(5)
α, deg	89.373(1)	90	90	90
β, deg	76.049(1)	132.156(1)	107.240(1)	106.461(1)
γ, deg	72.978(1)	90	90	90
V, Å^3; D_{calcd}, g cm^{-3}	565.42(3); 3.18	1233.49(14); 3.90	597.65(7); 4.02	656.25(6); 4.14
Diffractometer	Smart APEX II	Smart APEX II	Smart APEX II	Smart APEX I
Absorption correction	SADABS [17]	SADABS [17]	TWINABS [18]	SADABS [17]
μ(MoK_α), cm^{-1}	21.4	23.6	24.9	20.8
F(000), e	476	1240	620	692
hkl range	$-11 \le h \le +11$	$-29 \le h \le +29$	$-12 \le h \le +11$	$-12 \le h \le +11$
	$-15 \le k \le +15$	$-11 \le k \le +11$	$0 \le k \le +15$	$-15 \le k \le +14$
	$-16 \le l \le +16$	$-19 \le l \le +19$	$0 \le l \le +15$	$-14 \le l \le +14$
2θ range, deg	2.17 – 37.45	2.99 – 34.35	2.87 – 36.44	2.77 – 34.90
N_{all} / N'_{uniqe} / R_{int}	14375 / 5616 / 0.046	9408 / 2566 / 0.029	2913 / 2913 / 0	9896 / 2738 / 0.0253
Param. refined	122	62	62	62
Extinction coefficient	0.0078(4)	0.00089(8)	0.0032(3)	0.0038(2)
$R(F)_N$ / $R(F)_{N'}$ [a]	0.0435 / 0.0273	0.0318 / 0.0268	0.0420 / 0.0310	0.0272 / 0.0249
$wR(F^2)_N$ / $wR(F^2)_{N'}$ [a]	0.0719 / 0.0652	0.0730 / 0.0697	0.0775 / 0.0750	0.0613 / 0.0596
Weighting w: q_1 / q_2 [a]	0.0286 / 0	0.0411 / 1.0348	0.0453 / 0	0.0289 / 1.5474
GoF (F^2) [b]	0.973	1.057	0.988	1.040
$\Delta\rho_{fin}$ (max / min), e Å^{-3}	2.05 / −2.23	1.64 / −2.13	1.79 / −5.82	2.12 / −2.08
Deposition no.	CSD-419370	CSD-421656	CSD-421673	CSD-421657

[a] $R(F) = \Sigma||F_o| - |F_c||/\Sigma|F_o|$, $wR(F^2) = [\Sigma w(F_o^2 - F_c^2)^2/\Sigma w(F_o^2)^2]^{1/2}$, $w = [\sigma^2(F_o^2) + (q_1P)^2 + q_2P]^{-1}$, where $P = (\mathrm{Max}(F_o^2, 0) + 2F_c^2)/3$;
[b] GoF = $[\Sigma w(F_o 2 - F_c^2)^2/(n_{obs} - n_{param})]^{1/2}$.

In order to complete the consolidated findings and to learn more about the influence of the kind of alkali metal on the crystal structure we investigated the rubidium and cesium cyanoplatinate halides by X-ray crystal diffraction, differential thermal analysis (DTA), thermogravimetry (TG), and infrared (IR) and Raman spectroscopy.

Experimental Section

Synthesis

A concentrated aqueous solution of $Ba[Pt(CN)_4] \cdot 4\ H_2O$ (Chempur, 99.9 %) was added to excess amounts of aqueous solutions of Rb_2SO_4 (Sigma-Aldrich, 99.8 %) or Cs_2SO_4 (Alfa-Aesar, 99.99 %), as already described [12, 14]. After removing $BaSO_4$ by filtration, the respective halogen as chlorine gas, liquid bromine or an ethanolic solution of iodine was added to the clear filtrates containing rubidium or cesium tetracyanoplatinate, and boiled afterwards for one hour to remove the excess of halogen. Colorful needles of $Rb_2[Pt(CN)_4Cl_2]$ (green), $Rb_2[Pt(CN)_4Br_2]$ (yellow), $Rb_2[Pt(CN)_4I_2]$ (dark red), $Cs_2[Pt(CN)_4Cl_2]$ (light green), $Cs_2[Pt(CN)_4Br_2]$ (yellow), and $Cs_2[Pt(CN)_4I_2]$ (red) were grown by slowly concentrating the solutions by keeping them at r. t.

X-Ray structure determination

Single crystals of $Rb_2[Pt(CN)_4Cl_2]$, $Cs_2[Pt(CN)_4Br_2]$, $Rb_2[Pt(CN)_4I_2]$, and $Cs_2[Pt(CN)_4I_2]$ were selected under a microscope, and sealed in Lindemann glass capillaries. Their experimental intensity data were collected with graphite-monochromatized MoK_α radiation on a Smart APEX I (or APEX II) CCD diffractometer (Bruker AXS, Karlsruhe, Germany). The collection, done at 298(2) K, and reduction of data were carried out with the BRUKER SUITE software package [15]. $Rb_2[Pt(CN)_4Cl_2]$ crystallizes in the triclinic space group $P\bar{1}$ (no. 2), $Cs_2[Pt(CN)_4Br_2]$ monoclinically in $C2/c$ (no. 15), and $Rb_2[Pt(CN)_4I_2]$ and $Cs_2[Pt(CN)_4I_2]$ both monoclinically in $P2_1/c$ (no. 14). The structures were solved and refined using the program SHELXTL [16]. For $Rb_2[Pt(CN)_4Cl_2]$ and $Cs_2[Pt(CN)_4Br_2]$, the atomic positions of platinum, halogen and the alkali metal atoms were found by Direct Methods, and the positions of the cyanide groups were located from Difference Fourier maps. For

$Rb_2[Pt(CN)_4I_2]$ and $Cs_2[Pt(CN)_4I_2]$, the atomic coordinates of the isotypic $K_2[Pt(CN)_4I_2]$ [12] were used as starting model for the refinement. Such an approach was necessary, especially for $Rb_2[Pt(CN)_4I_2]$, because all crystals under investigation were systematically twinned (dove-tail twins), the volume ratio of the two twin components of the crystal under investigation being 0.907(1)/0.093(1). The intensities of all crystals were corrected for absorption effects applying a semi-empirical method [17, 18] (Table 1).

X-Ray powder diffraction data of $Cs_2[Pt(CN)_4Cl_2]$ (Fig. 1) were collected at r. t. using a Bruker D8 diffractometer in Debye-Scherrer geometry (primary beam Johannson-type Ge(220) monochromator for Mo$K_{\alpha 1}$ radiation, one-dimensional LynxEye PSD with silicon strips of 500 μm thickness and an opening angle of 3.5°) with the sample contained in a sealed borosilicate glass capillary of 0.2 mm diameter. Patterns were collected in the range $2\theta = 4 - 52°$ with a step width of 0.0085° in 2θ. There was no Bragg contribution to the pattern at angles higher than 50° in 2θ which was excluded from the analysis. The sample was spun during measurements for better particle statistics. For indexing and refinement of the powder pattern of $Cs_2[Pt(CN)_4Cl_2]$, the program TOPAS [19] was used. Indexing was performed by iterative use of singular value decomposition (LSI) [20], leading to the lattice parameters given in Table 2. The peak profiles and precise lattice parameters for all three phases were first determined by a LeBail fit [21] using the fundamental parameter (FP) approach of TOPAS [22]. Since the LynxEye and the Stoe PSD detectors are not fully described by the current implementation of the fundamental parameters approach in TOPAS, the instrument parameters were refined on respective measurements of a NIST standard material, SRM 660a (LaB_6) over the whole 2θ range of the instruments and used as starting values in the LeBail refinements. A cylindrical 2θ correction according to Sabine *et al.* [23] was applied. Starting values for the Rietveld refinement [24, 25] were taken from isostructural $Cs_2[Pt(CN)_4Br_2]$ in space group *C*2/*c* (see Tables 1 and 3). Due to the fact that free refinement of the atomic coordinates of the CN groups resulted in meaningless distortions, for the description of the $[Pt(CN)_4Cl_2]^{2-}$ octahedron a regular rigid body was constructed in the rigid body editor of TOPAS. The rigid body was defined in a way allowing for the refinement of the Pt–Cl, Pt–C (2×), and average C–N distances. Due to the fixed position of the rigid body at the origin of the unit cell, only three rotations for the $[Pt(CN)_4Cl_2]^{2-}$ octahedron as external degrees of freedom were subjected to global optimization. The structure giving the best fit to the data was validated by a Rietveld refinement. During the Rietveld refinement, the internal degrees of freedom as well as isotropic displacement parameters were refined.

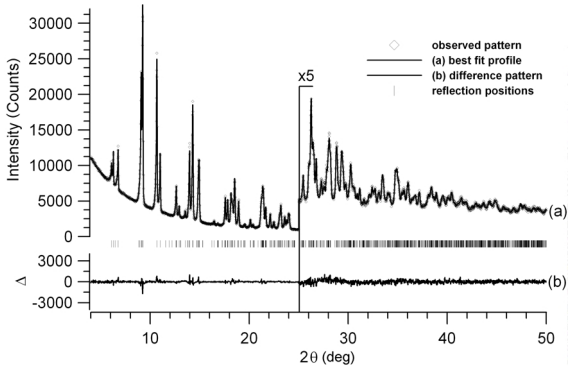

Fig. 1. Scattering X-ray intensities for $Cs_2[Pt(CN)_4Cl_2]$ at ambient conditions, as a function of the diffraction angle 2θ. Shown are the observed pattern (diamonds), the best Rietveld-fit profile (line a), the difference curve between observed and calculated profile (line b), and the reflection markers (vertical bars). The wavelength is λ = 0.7093 Å. The higher angle part of the plot is enlarged by a factor of five starting at $2\theta = 42°$.

Table 2. Crystallographic data of the powder structure refinement for $Cs_2[Pt(CN)_4Cl_2]$.

M_r, g mol^{-1}	535.67
Temperature, K	295
Space group (no.); Z	*C*2/*c* (15); 4
a, Å	17.947(4)
b, Å	7.395(2)
c, Å	12.031(3)
β deg	131.904(1)
V, Å^3; D_{calcd}, g cm^{-3}	1188.4(5); 3.55
Wavelength, Å	0.7093
R-exp, %[a]	1.93
R-p, %[a]	2.04
R-wp, %[a]	2.77
$R - F^2$, %[a]	1.20
GoF	1.44
θ range, deg	5.0 – 50.0
Step width, deg	0.0085
Time/scan, h	42
No. of variables	36
Deposition no.	CSD-421674

[a] R-exp, R-p, R-wp, and R-F^2 as defined in TOPAS (Bruker AXS GmbH) [19].

The crystallographic data of all compounds under investigation are collected in Tables 1 and 2, the positional and displacement parameters are listed in Table 3, selected atomic distances and angles are given in Tables 4 and 5.

Further details of the crystal structure investigations may be obtained from Fachinformationszentrum Karlsruhe, 76344 Eggenstein-Leopoldshafen, Germany (fax: +49-7247-808-666; e-mail: crysdata@fiz-karlsruhe.de, http://www.fiz-informationsdienste.de/en/DB/icsd/depot_anforderung.html) on quoting the deposition numbers given in Tables 1 and 2.

Physical properties

Differential thermal analysis (DTA) and thermogravimetry (TG) in combination with mass spectrometry (QMS 421,

Table 3. Atomic positions and equivalent isotropic displacement parameters U_{eq} (Å^2), with estimated standard deviations in parentheses.

Atom	Site	x	y	z	U_{eq}
$Rb_2[Pt(CN)_4Cl_2]$, $P\bar{1}$					
Pt1	1*a*	0	0	0	0.02225(5)
Pt2	1*h*	1/2	1/2	1/2	0.02003(4)
Rb1	2*i*	0.87406(6)	0.82270(4)	0.95215(4)	0.03855(9)
Rb2	2*i*	0.71063(6)	0.65796(4)	0.95215(4)	0.03730(9)
Cl1	2*i*	0.3214(1)	0.0205(1)	0.8572(1)	0.0362(2)
Cl2	2*i*	0.2582(2)	0.4709(1)	0.3760(1)	0.0358(2)
C11	2*i*	0.0672(5)	0.0758(4)	0.1727(4)	0.0287(6)
N11	2*i*	0.1077(6)	0.1190(4)	0.2682(4)	0.0454(8)
C12	2*i*	0.1523(6)	−0.2104(4)	0.0398(4)	0.0314(7)
N12	2*i*	0.2424(7)	−0.3286(4)	0.0635(5)	0.0493(9)
C21	2*i*	0.2838(6)	0.4992(4)	0.6842(3)	0.0284(6)
N21	2*i*	0.1634(6)	0.4899(4)	0.7861(4)	0.0450(8)
C22	2*i*	0.3936(6)	0.7259(4)	0.4936(4)	0.0307(7)
N22	2*i*	0.3424(7)	0.8516(4)	0.4853(5)	0.0505(9)
$Cs_2[Pt(CN)_4Cl_2]$, $C2/c$					
Pt1	4*a*	0	0	0	0.0197
Cs1	8*f*	0.1715(1)	0.4956(9)	0.0385(2)	0.0365
Cl1	8*f*	0.0735	0.2396	0.1738	0.0298
C1	8*f*	−0.0601	0.1733	−0.1616	0.0713
N1	8*f*	−0.0941	0.2712	−0.2530	0.0713
C2	8*f*	−0.1274	0.0142	−0.0251	0.0713
N2	8*f*	−0.1941	0.0217	−0.0382	0.0713
$Cs_2[Pt(CN)_4Br_2]$, $C2/c$					
Pt1	4*a*	0	0	0	0.02523(7)
Cs1	8*f*	0.18103(2)	0.49385(3)	0.03952(3)	0.04222(8)
Br1	8*f*	0.07197(3)	0.26460(5)	0.16893(4)	0.0417(1)
C1	8*f*	0.1209(3)	−0.0186(4)	0.0288(5)	0.0358(7)
N1	8*f*	0.1915(3)	−0.0349(6)	0.0500(6)	0.057(1)
C2	8*f*	0.0629(2)	−0.1743(5)	0.1669(4)	0.0382(7)
N2	8*f*	0.1016(3)	−0.2766(5)	0.2614(4)	0.060(1)
$Cs_2[Pt(CN)_4I_2]$, $P2_1/c$					
Pt1	2*a*	0	0	0	0.02380(6)
Cs1	4*e*	0.47802(4)	0.78147(3)	0.61611(3)	0.03687(7)
I1	4*e*	0.07943(4)	0.27477(3)	0.03036(3)	0.03754(7)
C1	4*e*	0.8061(5)	0.0265(4)	0.1036(4)	0.0298(6)
N1	4*e*	0.6916(6)	0.0423(5)	0.1586(5)	0.0432(8)
C2	4*e*	0.1837(5)	0.9612(4)	0.1969(4)	0.0298(6)
N2	4*e*	0.2935(5)	0.9382(4)	0.3058(4)	0.0398(7)
$Rb_2[Pt(CN)_4I_2]$, $P2_1/c$					
Pt1	2*a*	0	0	0	0.01674(6)
Rb1	4*e*	0.47700(7)	0.78204(6)	0.61738(5)	0.0330(1)
I1	4*e*	0.09041(4)	0.28164(3)	0.02936(4)	0.02912(8)
C1	4*e*	0.8003(6)	0.0333(5)	0.1053(5)	0.0231(8)
N1	4*e*	0.6805(7)	0.0529(6)	0.1591(5)	0.0353(9)
C2	4*e*	0.1934(6)	0.9601(5)	0.2028(5)	0.0220(7)
N2	4*e*	0.3089(6)	0.9358(5)	0.3140(4)	0.0308(8)

Balzers, Wiesbaden, Germany) for analyzing the volatile decomposition products were performed with a computer-controlled thermal analyzer (STA 409, Netzsch GmbH, Germany). Powder samples of 20 mg were placed in a corundum crucible, heated to 1173 K with a rate of 10 K min^{-1}, and then cooled down to r. t. with the same rate under argon.

The infrared spectra were recorded on an IR-Spectrometer (113v, Bruker, Germany) from 2 – 3 mg samples thoroughly mixed and ground with ∼400 mg of KBr (Aldrich, 99+ %, dried at 200 °C *in vacuo*) and subsequently pressed into pellets with a diameter of 13 mm.

The Raman spectra were measured by a laser with 0.4 W and a wavelength of 632 nm in a Confocal Microscope Laser Raman System (Model LabRam 1, Jobin-Yvon, France).

Results and Discussion

Crystal structures

The six representatives with the general formula $A_2[Pt(CN)_4X_2]$ (A = Rb, Cs; X = Cl, Br, I) crystallize in three different types of structures: $Rb_2[Pt(CN)_4Cl_2]$ (Fig. 2) crystallizes in the triclinic space group $P\bar{1}$; $Rb_2[Pt(CN)_4I_2]$ (Fig. 3) and $Cs_2[Pt(CN)_4I_2]$ crystallize in the already known $Rb_2[Pt(CN)_4Br_2]$-type structure (monoclinic space group $P2_1/c$) [11], which is also realized by $K_2[Pt(CN)_4X_2]$ (X = Cl, Br, I) [12], and

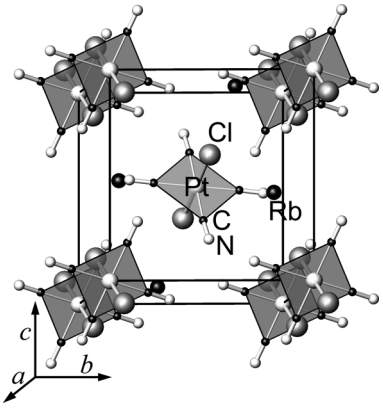

Fig. 2. Perspective representation of the crystal structure of $Rb_2[Pt(CN)_4Cl_2]$, with the margins of the unit cell (black).

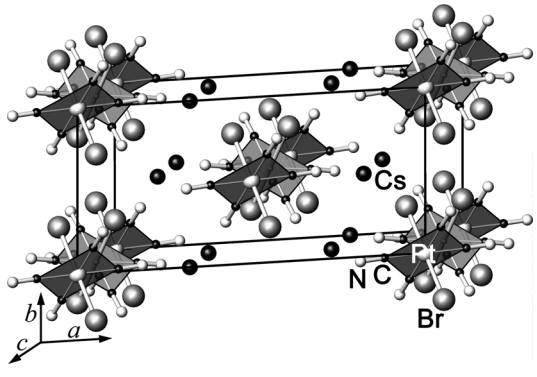

Fig. 3. Perspective representation of the crystal structure of $Cs_2[Pt(CN)_4Br_2]$, with the margins of the unit cell (black).

Table 4. Selected distances (Å) and angles (deg) of $Rb_2[Pt(CN)_4Cl_2]$ with estimated standard deviations in parentheses.

Atom		Distance	Atom		Distance	Atom	Angle
Pt1	–C11	2.019(3) × 2	Pt2	–C22	2.020(4) × 2	C11–Pt1–C12	91.5(2)
	–C12	2.012(3) × 2		–C21	2.017(3) × 2	C21–Pt2–C22	87.0(2)
	–C*l*1	2.3399(9) × 2		–C*l*2	2.3267(9) × 2	Pt1–C11–N11	178.8(4)
Rb1	–C*l*1	3.484(1)	Rb2	–C*l*1	3.459(1)	Pt1–C12–N12	178.3(3)
	–C*l*2	3.490(1)			3.885(1)	Pt2–C21–N21	175.9(3)
		3.511(1)		–C*l*2	3.342(1)	Pt2–C22–N22	176.9(3)
	–N11	3.016(3)		–N12	2.993(4)	C*l*1–Pt1–C11	90.2(1)
	–N22	2.983(4)			3.061(4)	C*l*1–Pt1–C12	90.5(1)
		3.430(5)		–N21	3.051(4)	C*l*2–Pt2–C21	88.8(1)
		3.442(5)			3.051(4)	C*l*2–Pt2–C22	88.8(1)
C11	–N11	1.134(5)	C21	–N21	1.139(5)		
C12	–N12	1.142(5)	C22	–N22	1.128(5)		

Table 5. Selected distances (Å) and angles (deg) with estimated standard deviations in parentheses.

		$Rb_2[Pt(CN)_4I_2]$	**$Cs_2[Pt(CN)_4Cl_2]$**	**$Cs_2[Pt(CN)_4Br_2]$**	**$Cs_2[Pt(CN)_4I_2]$**
Pt1	–C1	2.014(5) × 2	1.95(3) × 2	2.007(4) × 2	2.010(4) × 2
	–C2	2.010(4) × 2	2.10(2) × 2	2.006(4) × 2	2.008(4) × 2
	–*X*	2.6829(3) × 2	2.360(8) × 2	2.4773(4) × 2	2.6879(3) × 2
A	–N1	3.043(5)	3.178(4)	3.214(5)	3.168(4)
		3.235(5)	3.714(4)	3.435(4)	3.214(4)
		3.418(5)	3.929(3)	3.853(4)	3.311(4)
	–N2	3.022(5)	3.11(3)	3.129(4)	3.242(4)
		3.031(4)	3.593(7)	3.566(4)	3.406(5)
		3.187(5)	3.920(2)	4.175(4)	3.466(5)
	–*X*	3.8273(6)	3.628(4)	3.7049(5)	4.0059(4)
		3.8601(6)	3.876(3)	3.9454(5)	4.0475(4)
		4.0237(7)	3.983(4)	3.9870(5)	4.1060(4)
C1	–N1	1.151(6)	1.10(2)	1.146(6)	1.143(5)
C2	–N2	1.139(6)	1.10(2)	1.146(6)	1.146(5)
C1–Pt1–C2		89.1(2)	90	91.7(2)	89.7(2)
Pt1–C1–N1		177.0(4)	180	176.9(6)	177.9(4)
Pt1–C2–N2		176.7(4)	180	176.9(3)	177.1(3)
X–Pt1–C1		90.1(1)	90	89.8(1)	90.1(1)
X–Pt1–C2		90.2(1)	90	90.4(1)	89.8(1)

finally, the two isotypic compounds $Cs_2[Pt(CN)_4Cl_2]$ and $Cs_2[Pt(CN)_4Br_2]$ (Fig. 4) crystallize also in the monoclinic system but in space group *C*2/*c*, *c. f.* Tables 1 – 3.

In all alkali metal tetracyanoplatinate halides mentioned above, the platinum(IV) atoms are in an octahedral coordination. The carbon atoms of the cyanide groups provide a square-planar basis, and the halogen atoms are located in the axial (*trans*) positions of the $[Pt(CN)_4X_2]^{2-}$ octahedron. The bond lengths Pt–C and C–N correspond to the expected values. A slight decrease of both lengths is observed from the iodine to the chlorine compounds, which correlates with increasing of IR vibrational frequencies (Tables 4 and 5).

The arrangement of the platinum atoms, as the centers of the octahedra, is body-centered *I* in $Rb_2[Pt(CN)_4Cl_2]$ (Fig. 2), showing the same arrangement as in the *F* centered K_2PtCl_6 structure type [26], with $b\sqrt{2} \approx c\sqrt{2} \triangleq a(K_2PtCl_6)$. In the case of the other representatives a face-centered arrangement is observed: $Cs_2[Pt(CN)_4Cl_2]$ and $Cs_2[Pt(CN)_4Br_2]$ face-centered *C* (Fig. 3); $Rb_2[Pt(CN)_4I_2]$ and $Cs_2[Pt(CN)_4I_2]$ face-centered *A* (Fig. 4).

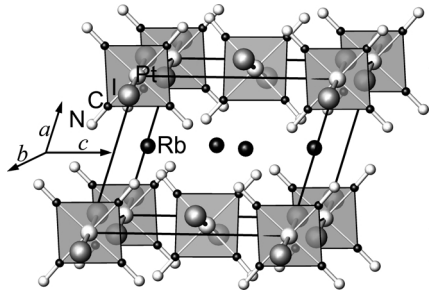

Fig. 4. Perspective representation of the crystal structure of $Rb_2[Pt(CN)_4I_2]$, with the margins of the unit cell (black).

Table 6. IR vibrational frequencies (cm^{-1}) of $A_2[Pt(CN)_4X_2]$ (A = Rb, Cs; X = Cl, Br, I)[a].

	$Rb_2[Pt(CN)_4Cl_2]$	$Rb_2[Pt(CN)_4Br_2]$	$Rb_2[Pt(CN)_4I_2]$
ν(C≡N)	2174 vs	2170 vs	2159 vs
ν(Pt–C)	492 s, 477 s	494 s, 476 s	490 s, 473 s
δ(Pt–C≡N)	403 s	404 s	405 s
	$Cs_2[Pt(CN)_4Cl_2]$	$Cs_2[Pt(CN)_4Br_2]$	$Cs_2[Pt(CN)_4I_2]$
ν(C≡N)	2171 vs	2166 vs	2158 vs, 2129 s
ν(Pt–C)	487 s, 468 s	487 s, 471 s	490 s
δ(Pt–C≡N)	408 vs	409 vs	407 s

[a] vs = very strong, s = strong, w = weak.

Table 7. Raman vibrational frequencies (cm^{-1}) of $A_2[Pt(CN)_4X_2]$ (A = Rb, Cs; X = Cl, Br, I)[a].

	$Rb_2[Pt(CN)_4Cl_2]$	$Rb_2[Pt(CN)_4Br_2]$	$Rb_2[Pt(CN)_4I_2]$
ν(C≡N)	2196 s	2192 s	2185 s
	2187 w	2184 w	2174 w
ν(Pt–C)	469 s	468 s	467 s
ν(Pt–X)	327 vs	198 vs	149 s
δ(Pt–C≡N)	151 vs	146 vs	140 vs
	$Cs_2[Pt(CN)_4Cl_2]$	$Cs_2[Pt(CN)_4Br_2]$	$Cs_2[Pt(CN)_4I_2]$
ν(C≡N)	2197 s	2193 s	2186 s
	2187 w	2183 w	2175 w
ν(Pt–C)	472 s	469 s	471 w
ν(Pt–X)	333 vs	204 vs	143 vs
δ(Pt–C≡N)	150 s	143 s	140 vs

[a] vs = very strong, s = strong, w = weak.

Thermogravimetric analysis

The thermal decomposition of $Cs_2[Pt(CN)_4Br_2]$, measured exemplarily by DTA and TG-MS, starts with a separation of part of the cyanide at 300 °C. At higher temperature, the CN^- and $(CN)_2$ groups and halogen are evolved progressively, until elemental platinum is left as the only solid residue. All other rubidium and cesium cyanoplatinate halides $A_2[Pt(CN)_4X_2]$ (A = Rb, Cs; X = Cl, Br, I) behave similarly, thus corresponding to the potassium cyanoplatinate halides investigated previously [12].

Infrared spectroscopy

The infrared spectra (Table 6) of all alkali metal cyanoplatinate halides $A_2[Pt(CN)_4X_2]$ (A = Rb, Cs; X = Cl, Br, I) show a sharp strong absorption band for A = Rb at 2159 cm^{-1} (X = I), 2170 cm^{-1} (X = Br) or 2174 cm^{-1} (X = Cl), and for A = Cs at 2158 cm^{-1} (X = I), 2166 cm^{-1} (X = Br) or 2171 cm^{-1} (X = Cl), which are assigned to the valence vibration of the C≡N groups [27]. With increasing size and decreasing electronegativity of the halogen atoms the frequencies ν(C≡N) are shifted to lower values, but are still above the ν(C≡N) values of cyanoplatinates(II) like $Rb_2[Pt(CN)_4]$ (2132 cm^{-1}) [28]. The charge of the platinum atom of the complex has a significant influence on the C≡N bonding character, whereas the type of cation has only a marginal influence. The strong bands at 487 to 494 cm^{-1} and 468 to 477 cm^{-1} are assigned to the valence vibrations of the Pt–C bonds [28]. The absorption band of the deformation vibration of the Pt–C≡N groups occurs at 403 to 409 cm^{-1} [39, 30].

Raman spectroscopy

The Raman spectra (Table 7) of all representatives of the type $A_2[Pt(CN)_4X_2]$ with A = Rb, Cs, and X = Cl, Br, I show two bands of the ν(C≡N) vibration between 2174 and 2197 cm^{-1} [31] with decreasing frequencies, depending on the halogen atom, from X = Cl to I. The electronegativity effect of the halogen atoms on the force constants of the Pt–C bonds at frequencies of 467 to 472 cm^{-1} and on the δ(Pt–C≡N) deformation vibrations, decreasing from 151 cm^{-1} (X = Cl) to 140 cm^{-1} (X = I) in both cyanoplatinate halides, is not very pronounced. The bands of the ν(Pt–X) vibration have a very high intensity as observed in the potassium tetracyanoplatinate halides [12] and occur for A = Rb at 149 cm^{-1} (X = I), 198 cm^{-1} (X = Br) and 327 cm^{-1} (X = Cl), and for A = Cs at 143 cm^{-1} (X = I), 204 cm^{-1} (X = Br) and 333 cm^{-1} (X = Cl). Again, the frequencies decrease with the increasing size and the decreasing electronegativity of the halogen atoms, but are not affected by the cation size.

Acknowledgement

The authors would like to thank W. König for the IR, A. Schulz for the Raman and Th. Pilz for the DTA/TG measurements.

[1] W. Knop, G. Schnedermann, *J. Prakt. Chem.* **1846**,*37*, 461.
[2] K. Krogmann, *Angew. Chem.* **1969**, *81*, 10 – 17; *Angew. Chem., Int. Ed. Engl.* **1969**, *8*, 35 – 42.
[3] K. Krogmann, H. D. Hausen, *Z. Naturforsch*. **1968**, *23b*, 1111.
[4] H. R. Zeller, *Festkörperprobleme*, Vol. 13, Pergamon Press Ltd., New York, **1973**, pp. 31 – 58.
[5] J. M. Williams, *Adv. Inorg. Chem*. **1983**, *26*, 235 – 268.
[6] J. M. Williams, R. K. Brown, *Inorg. Chem*. **1978**, *17*, 2607 – 2609.

[7] J. M. Williams, P. L. Johnson, A. J. Schultz, C. C. Coffey, *Inorg. Chem*. **1978**, *17*, 834 – 839.
[8] J. M. Williams, D. J. Wood, A. E. Underhill, *Solid State Commun.* **1979**, *31*, 219 – 221.
[9] B. M. Anderson, S. K. Hurst, *Eur. J. Inorg. Chem.* **2009**, 3041 – 3054.
[10] J. M. Williams, P. L. Johnson, T. R. Koch, *Acta Crystallogr.* **1977**, *B33*, 558 – 560.
[11] J. M. Williams, G. Needham, P. Johnson, T. L. Cornish, *Acta Crystallogr.* **1977**, *B33*, 887 – 889.
[12] C. Mühle, A. Karpov, J. Nuss, M. Jansen, *Z. Naturforsch*. **2004**, *59b*, 567 – 572.
[13] C. Mühle, E.-M. Peters, M. Jansen, *Z. Naturforsch.* **2009**, *64b*, 111 – 115.
[14] J. M. Williams, T. R. Koch, P. L. Johnson, *Inorg. Chem.* **1977**, *16*, 640 – 645.
[15] BRUKER SUITE (version 2008/3), Bruker Analytical X-ray Instruments Inc., Madison, Wisconsin (USA) **2008**.
[16] G. M. Sheldrick, *Acta Crystallogr.* **2008**, *A64*, 112 – 122.
[17] G. M. Sheldrick, SADABS (version 2008/1), Program for Empirical Absorption Correction of Area Detector Data, University of Göttingen, Göttingen (Germany) **2008**.
[18] G. M. Sheldrick, TWINABS (version 2008/4), Bruker AXS Scaling for Twinned Crystals, University of Göttingen, Göttingen (Germany) **2008**.
[19] TOPAS (version 4.1), General Profile and Structure Analysis Software for Powder Diffraction Data, Bruker AXS GmbH, Karlsruhe (Germany) **2008**.
[20] A. A. Coelho, *J. Appl. Crystallogr.* **2000**, *33*, 899 – 908; A. A. Coelho, *J. Appl. Crystallogr.* **2003**, *36*, 86 – 95.
[21] A. Le Bail, H. Duroy, J. L. Fourquet, *Mater. Res. Bull.* **1988**,*23*, 447 – 452.
[22] R. W. Cheary, A. A. Coelho, J. P. Cline, *J. Res. Natl. Inst. Stand. Technol.* **2005**, *109*, 1 – 25.
[23] T. M. Sabine, B. A. Hunter, W. R. Sabine, C. J. Ball, *J. Appl. Crystallogr*. **1998**,*31*, 47 – 51.
[24] H. M. Rietveld, *Acta Crystallogr.* **1967**, *22*, 151 – 152; H. M. Rietveld, *J. Appl. Crystallogr.* **1969**, *2*, 65 – 71.
[25] F. Izumi in *The Rietveld Method* (Ed.: R. A. Young), Oxford University Press, Oxford, **1993**, chapter 13.
[26] R. J. Williams, D. R. Dillin, W. O. Milligan, *Acta Crystallogr.* **1973**, *B 29*, 1369 – 1372.
[27] C. Várhelyi, I. Ganescu, *Studia Univ. Babes-Bolyai*, *Chemia* **1991**, *XXXVI 1 – 2*, 8 – 14.
[28] C. Mühle, A. Karpov, M. Jansen, *Z. Naturforsch*. **2005**,*60b*, 1269 – 1272.
[29] C. Mühle, J. Nuss, R. E. Dinnebier, M. Jansen, *Z. Anorg. Allg. Chem*. **2004**, *630*, 1462 – 1468.
[30] L. H. Jones, J. M. Smith, *Inorg. Chem.* **1965**, *4*, 1677 – 1681.
[31] J. M. Williams, J. L. Petersen, H. M. Gerdes, S. W. Peterson, *Phys. Rev. Lett.* **1974**, *33*, 1079 – 1081.